# Tracking the deformation history of a high-position landslide: satellite-based analysis of the 24 June 2017 Xinmo landslide in Sichuan, China

A catastrophic landslide occurred on Mount Fugui, Diexi Town, Mao County, Northern Sichuan Province, China on 24 June 2017 (32°04′09.4″N, 103°39′03.4″E; Figure 1 a), which destroyed the Xinmo village, resulting in 83 casualties. The trailing edge of the Xinmo landslide was located on the ridge of Mount Fugui (Figure 1 b). Based on spatial position and movement of the slide body, the landslide area was divided into the sliding source zone, landslide runout zone and accumulation zone (Figure 1 c and d). The slope angle, elevation difference, horizontal distance, and total volume of the landslide were 53°, 1200 m, 2800 m and $1.7 \times 10^7 \, m^3$ respectively. The apparent friction angle (i.e. angle between the back edge of the landslide and the farthest horizontal extent) was ~23° (Figure 1 e). Since Mount Fugui is located in the Longmenshan fault zone, it experiences earthquakes frequently[1,2]. It is a shattering mountain that formed in the epicentre area of the *Ms* 7.5 earthquake (intensity X) in 1933 and the strong motion area of the *Ms* 8.0 Wenchuan earthquake (intensity IX) in 2008. In 2017, the total rainfall in the town of Songpinggou, in which the landslide was located, exceeded 227.4 mm. The Xinmo landslide occurred due to the combined action of the broken rock mass, rainfall and steep slope, it was a typical high-position and long-runout landslide. This type of landslide exhibits the following characteristics: large elevation difference (generally >500 m), high speed (generally >20 m/s) and destructiveness[3]. In recent years, due to the casualties and economic losses caused by high-position and long-runout landslides, they have been classified as ecological disasters[4,5]. Furthermore, it is particularly important to identify the geological hazards of high-position landslides during their early stage. Together, these approaches help provide a reference for local governments to define dangerous areas, take necessary measures (e.g. resettlement and activation of early-warning systems), and formulate development plans for the endangered areas[6].

High-position landslides generally occur in mountain–canyon regions, and fracture development is a typical sign of an impending landslide. The fractures commonly develop on mountain ridges. Owing to vegetation coverage and high altitude, the fracture development area is usually not visible. It is challenging for researchers and instruments to reach the fracture area, which makes it more difficult to identify the geological hazards of a high-position landslide during its early stage. In recent years, remote sensing images are an effective tool for evaluating the deformation process of
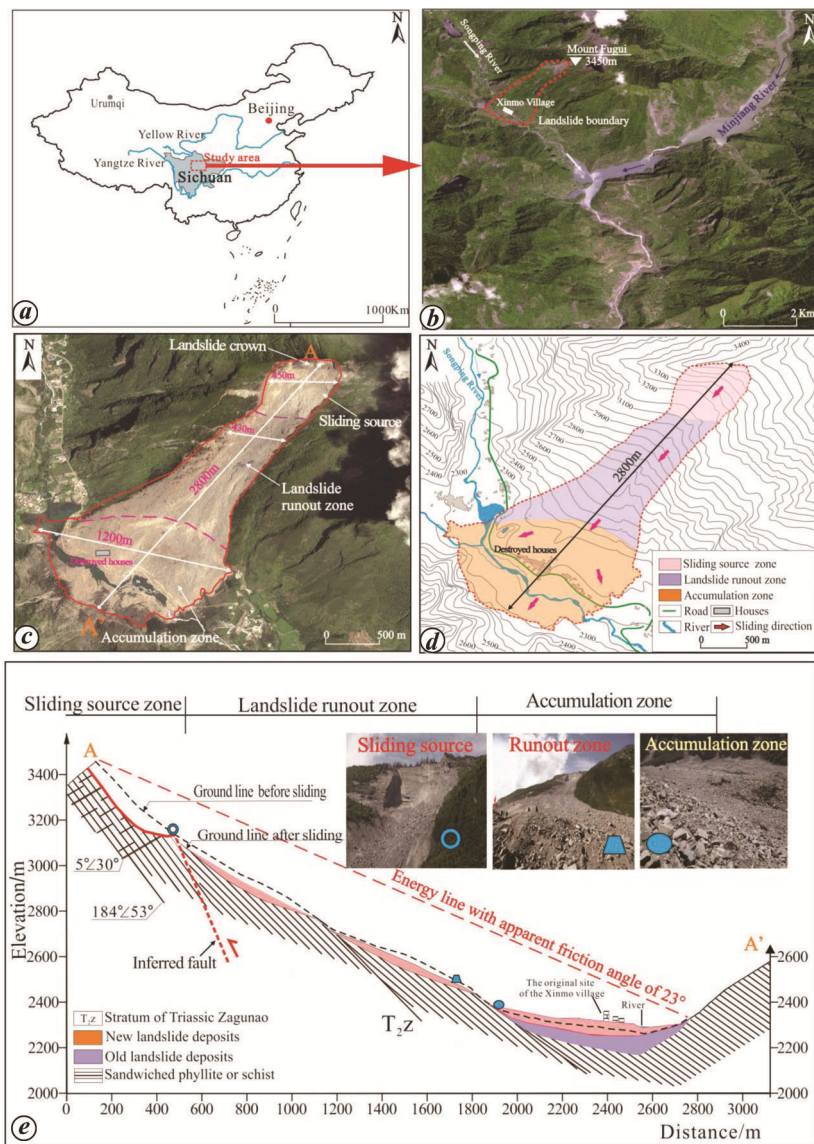
Figure 1. *a*, Location of the Xinmo landslide at Maoxian, Sichuan Province, China. *b*, Terrain and landforms of the study area. *c*, Overview after sliding and characteristics of the Xinmo landslide. *d*, Topographic contour map showing zones of the sliding source zone, landslide runout zone and accumulation zone. *e*, Longitudinal profile of the Xinmo landslide. The energy line is indicated from the back edge of the landslide and the farthest horizontal extent with an angle of 23°.

landslides[7,8]. Based on the analysis of historical remote sensing images of the Xinmo landslide, its entire formation process was inverted using the visual interpretation method. IKONOS satellite images taken on 27 July 2005 revealed that five fractures had formed in the area at elevation ranging from 3400 to 3500 m (Figure 2 *a* and *b*). The average width of the fractures was ~5 m and the maximum length was ~100 m. The fracture direction was perpendicular to the ridge direction and there was some talus in the area at 3200–3430 m elevation and a volume of 7×10^4 m³. Analysis of pre-event QuickBird satellite imagery (22 June 2013) showed that further cracks had developed, resulting in rock mass structure fractures and an increase in the talus

volume to 30×10^4 m³ (Figure 2 *c* and *d*). According to satellite images of the landslide source zone from 2013 to 2017 (Figure 3), the cracks extended farther. Specifically, cracks 1 and 4 extended tens of metres, were continuously distributed and comparatively developed on the east and west sides of the sliding source area. This defined the lateral separation boundary of the landslide. The front end of the talus was in contact with the gully (Figure 2 *e* and *g*). According to local villagers, the gully was cut to a depth >1 m by flows, indicating that the interaction between surface water and pore water was strong.

Based on field geological survey, multi-temporal remote sensing images and indoor testing, the triggering mechanisms

of the Xinmo landslide were analysed. The analysis revealed that the main inducing factors of the landslide were the structure of the rock mass, earthquakes and rainfall. Also, there were three main disaster-inducing stages.

During the first stage, the rock was severed into a grid. The stratum structure of the Xinmo landslide is a flysch formation, which is composed of an interbedded structure of sandstone and slate (Figure 4 *c*). Due to the significant impact of multi-phase tectonic movement, the rock mass exhibited a thick plate-like undulating deformation. The thickness of a single bed was 3–5 m. The strata displayed an undulating deformation as a result of compression. The steep-dip structural planes, such as phyllite and
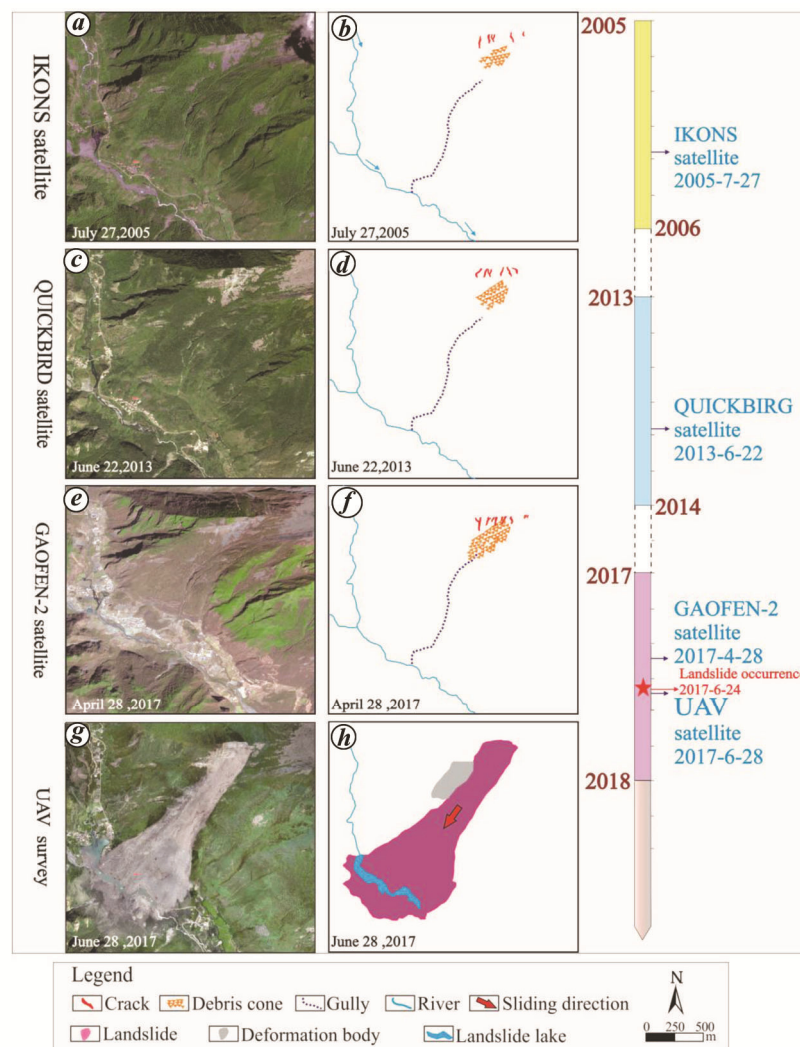
Figure 2. Comparison of multi-temporal remote sensing images of the Xinmo landslide: *a*, 27 July 2005 (IKONS, $R = 1.0$ m). *c*, 22 June 2013 (QuickBird, $R = 0.61$ m). *e*, 28 April 2017 (Gaofen-2, $R = 0.8$ m). *g*, 28 June 2017 (UAV image, $R = 1$ m). *b*, *d*, *f*, Geometric sketches depicting fracture development and talus distribution at different times: *b*, 27 July 2005. *d*, 22 June 2013. *f*, 28 April 2017. *h*, Geometric sketch depicting scope of the landslide.

1743
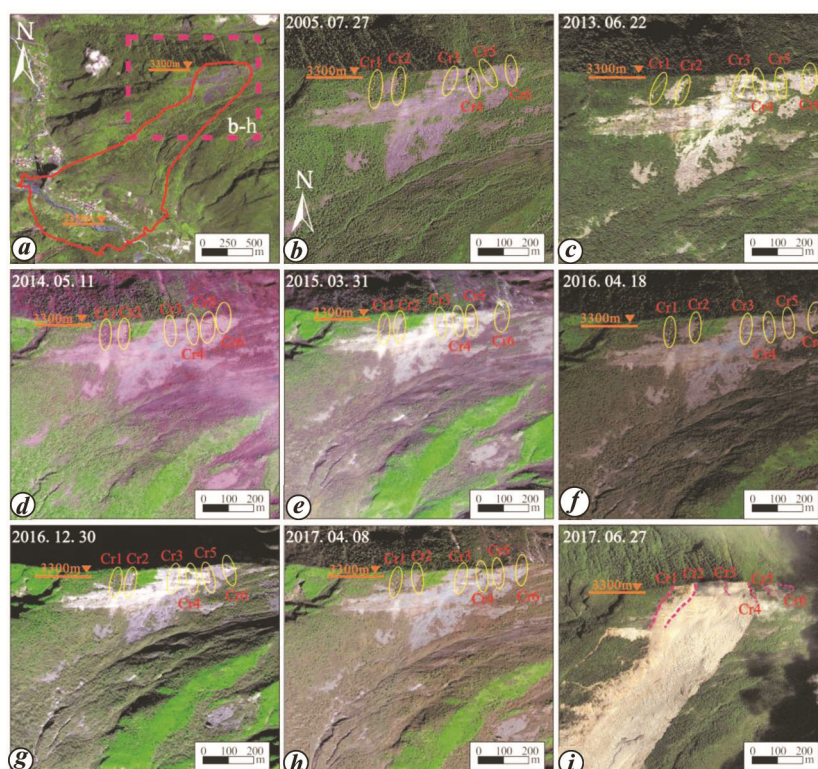
Figure 3. Satellite images showing crack development based on multi-temporal remote sensing of the landslide source zone: ***a***, Boundary of the landslide source zone (dotted line; 27 July 2005). ***b***, 27 July 2005. ***c***, 22 June 2013. ***d***, 11 May 2014. ***e***, 31 March 2015. ***f***, 18 April 2016. ***g***, 30 December 2016. ***h***, 8 April 2017. ***i***, 27 June 2017. ((***a***)–(***i***) are from the Gaofen-2 satellite; $R = 0.8$ m.)

slate, constituted a weak sliding zone. There were some preferred structural planes in the mountains of the attitude of the structural planes 350° ∠40°, where the joint zone was opposite that of the rock inclination. In addition, a blocky and consequently slippery geologic structure was formed due to the cutting and separating effects of multiple groups of discontinuous structural surfaces (Figure 4 c). In addition, there were two continuously distributed, large, anti-dip joint fracture zones in the landslide source area, which provided bulging deformation and sliding of the fractured rock mass (Figure 4 c).
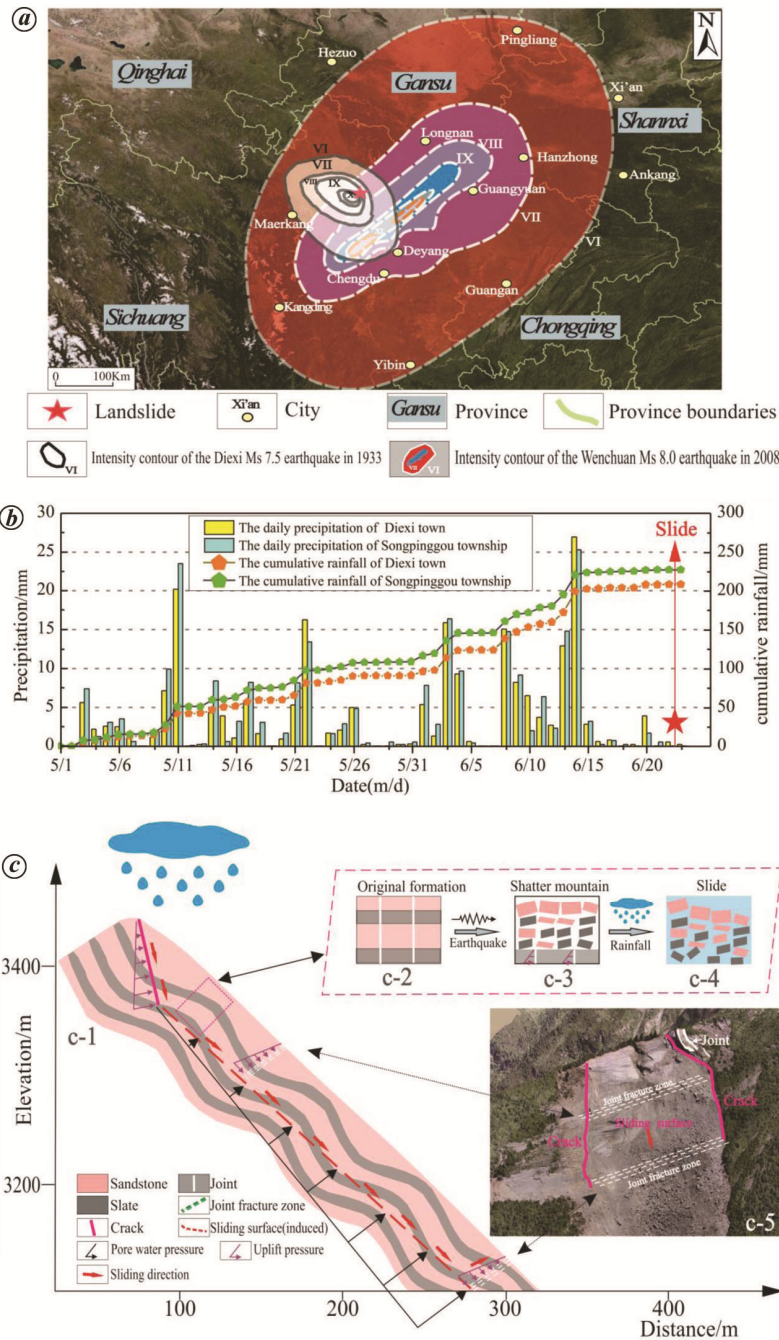
The shattered mountains formed during the second stage. The earthquake in the region has the characteristic of high intensity. After the Wenchuan earthquake, in the middle of the sliding source area, a group of dense, longitudinal, tensile, fissure zones had formed, running nearly parallel to the slope inclination, which increased the amount of rock damage and fracture. This further confirmed that the vibration amplification

effect of the magnitude 8.0 Wenchuan earthquake along the fault zone was significant[2].

The third and final stage was the occurrence of the landslide under the action of rainfall. Heavy sustained rainfall occurred in this area from 8 to 14 June 2007, during which the cumulative precipitation reached approximately 80 mm (Figure 4 b). Rainwater infiltrated the rock mass through visible fracture cracks. The emergence strata in Mount Fugui consist of metamorphic quartz sandstone with slate. Indoor testing revealed that the sandstone density, saturation tensile strength testing index, saturation compressive strength testing index and softening coefficient were approximately 2700 kg/m³, 107 MPa, 1.4 MPa and 0.79 respectively. The slate density, saturation tensile strength testing index, saturation compressive strength testing index and softening coefficient were approximately 2640 kg/m³, 56 MPa, 1.2 MPa and 0.72 respectively. This type of rock is prone to weakening due to rainwater infiltration. In addition, hydro-

static pressure in the cracks increased due to rainfall. As a result of the uplift pressure, lateral water pressure and softening of the fractured rock mass in the landslide source zone, the sliding surfaces merged and the landslide occurred.

At present, the early identification of high-position landslides is a hot research topic. In this study, a method for observing the deformation process of high landslide hazards by analysing multi-period remote sensing images, which is a qualitative prediction method, has been introduced. Analysing multi-period remote sensing images helps in the analysis of the evolutionary process of landslides[9]. These images could also help define the boundaries of dangerous areas. The deformation characteristics of dangerous areas were evaluated using a variety of monitoring techniques (e.g. synthetic aperture radar interferometry [InSAR] and offset tracking). When utilizing InSAR and offset-tracking technology to quantitatively analyse displacement change of the deformation area, the accuracy can reach the millimetre level.

2. Yin, Y. P., Wang, W. P., Zhang, N., Yan, J. K., Wei, Y. J. and Yang, L. W., *Geology China*, 2017, **44**(5), 827–841 (in Chinese).
3. Hungr, O., Leroueil, S. and Picarelli, L., *Landslides*, 2013, **11**(2), 167–194; doi:10.1007/s10346-013-0436-y.
4. Klimeš, J., Rosario, A. M., Vargas, R., Raška, P., Vicuña, L. and Jurt, C., *Landslides*, 2019; doi:10.1007/s10346-019-01203-w.
5. Zhang, Y., Xing, A., Jin, K., Zhuang, Y., Bilal, M., Xu, S. and Zhu, Y., *Landslides*, 2020; doi:10.1007/s10346-020-01436-0.
6. Hungr, O., *KSCE J. Civ. Eng.*, 2009, **13**(4), 281–287; doi:10.1007/s12205-009-0281-7.
7. Willenberg, H., Eberhardt, E., Loew, S., McDougall, S. and Hungr, O., *Landslides*, 2009, **6**(2), 111–119; doi:10.1007/s10346-009-0146-7.
8. Roy, P., Martha, T. R., Jain, N. and Kumar, K. V., *Curr. Sci.*, 2018, **115**(3), 395–398.
9. Zhao, C. and Lu, Z., *Remote Sensing*, 2018, **10**, 279; doi:10.3390/rs10020279.

LONGWEI YANG[1,2,]*
SAINAN ZHU[2]
WENPEI WANG[2]
NAN ZHANG[2]
YUNJIE WEI[2]
FEIHANG QU[3]

[1]*School of Geological Engineering and Geomatics,*
Chang'an University,
Xi'an 710054, China
[2]*China Institute of Geo-Environment Monitoring,*
CGS,
Beijing 100081, China
[3]*Shaanxi Geology and Mining Geophysical and Geochemical Prospecting Team Co Ltd,*
Xi'an 710043, China
*For correspondence.
e-mail: yang0504@chd.edu.cn*

Figure 4. *a*, Regional seismic intensity map of the landslide. *b*, Plot of rainfall in Xinmo village from 1 May to 23 June 2017. *c*, Failure mode and hydrogeological characteristics of the landslide source zone.

Moreover, observations were carried out using ground-based laser scanning technology. Since such mapping is not affected by vegetation, this technology can accurately delineate the landslide risk area and provide an accurate three-dimensional terrain model for numerical simulation analysis. A crack meter, rain gauge and other monitoring instruments were installed in the deformation area in order to transmit the displacement and deformation data of the deformation area in real time, thereby achieving the early monitoring and early warning of high-position landslide geological disasters. This is the future research direction for the early observation and monitoring systems of such disasters.

1. Fan, X. *et al.*, *Eng. Geol.*, 2018, **241**, 25–32.